Dry Metal Forming Open Access Journal

Fast Manuscript Track

Edited by Frank Vollertsen
Available online elib.suub.uni-bremen.de

www.drymetalforming.de

Dry Met. Forming OAJ FMT 3 (2017) 081–089
Received 10 May 2017; published 30 May 2017

Mechanical and tribological characterization of self-lubricating $(Cr_{1-x}Al_x)N$ coatings for deposition on complex-shaped forging tools

Kirsten Bobzin[1], Tobias Brögelmann[1], Nathan C. Kruppe[1], Mostafa Arghavani*[1], Dennis C. Hoffmann[1], Fritz Klocke[2], Patrick Mattfeld[2], Daniel Trauth[2], Rafael Hild[2]

[1]Surface Engineering Institute (IOT), RWTH Aachen University, Kackertstr. 15, 52072 Aachen, Germany
[2]Laboratory for Machine Tools and Production Engineering (WZL), RWTH Aachen University, Steinbachstr. 19, 52074 Aachen, Germany

Abstract

Cold forging processes in production engineering enable a high material utilization with a considerable energy and resource efficiency. In such processes, liquid and solid lubricants are commonly used to reduce the friction between forming tools and workpieces. However, using of lubricants in tribological cold forging processes is unfavorable to economic, ecological and legislative perspectives. To overcome disadvantages of lubricants and conduct lubricant-free cold forging, the physical vapor deposition (PVD) technology for coating of metal forming tools can be applied. Such coatings contain soft and hard constituents. Self-lubricating systems such as MoS_2 will be applied as soft constituents. Furthermore, incorporation of MoS_2 into the hard matrixes such as $(Cr_{1-x}Al_x)N$ is required, in order to increase the life time of coated tools under high tribological loads in dry cold forging. In the presented work, self-lubricating coatings in system $(Cr_{1-x}Al_x)N+MoS_y$ with two different nitrogen contents for the application in dry cold forging of steel were investigated. The coatings were deposited on tool steel X155CrMoV12 (DIN 1.2379, AISI D2) using a hybrid technology, consisting of direct current and high power pulse magnetron sputtering dcMS/HPPMS in an industrial scale PVD unit. In order to investigate the distribution of coating thickness s along the length of complex-shaped forging tools L_{tool}, an experimental tool was designed and the aspect ratio s/L_{tool} was determined. The coating and substrate/coating compound properties were investigated. Tribological model tests were conducted using a pin-on-disc (PoD) tribometer, which simulates dry contacts in cold forging. The analyses were performed using pins made of 16MnCr5 (DIN 1.7131, AISI 5115) and included the determination of friction coefficients. Furthermore, contact region was studied by Raman spectroscopy after the tribological tests. Based on the results, the coating system $(Cr_{1-x}Al_x)N+MoS_y$ exhibits a high potential for application in dry cold forging of steel. Moreover, an increase of nitrogen content in the coatings leads to an enhancement of adhesion strength between substrate and coating and the tribological behavior of the coated tools against 1.7131.

Keywords: cold forging, PVD, hybrid-dcMS/HPPMS, tribology, $(Cr_{1-x}Al_x)N+MoS_y$

1 Introduction

Cold forging processes in production engineering are of great importance due to their potential for high material utilization and considerable energy and resource efficiency [1]. In order to reduce friction between forming tools and workpieces during the cold forging, different types of liquid or solid lubricants are used. However, due to economic reasons as well as high demands for environmentally friendly metal forming process, there is a huge interest in lubricant-free cold forging [2-6].

Self-lubricating tool coatings deposited by physical vapor deposition (PVD) can be applied as alternatives for the lubricants in cold forging processes. Such coatings contribute to a reduction of friction forces between forming tools and workpieces and therefore, to a reduced wear rate of tools. The self-lubricating character of these PVD coatings is based on coating's constituents with extreme low coefficient of friction (CoF), e.g. transition metal dichalcogenides (TMD) [7-11]. Molybdenum disulfide (MoS_2) and tungsten disulfide (WS_2) are two types of TMDs, which are

*E-mail address of corresponding author: basturk@iot.rwth-aachen.de

increasingly in the focus of attention in this area of research [12-16]. In such TMDs, the crystallographic layers are bonded together with relatively weak van der Waals forces. This leads to a low shear strength and, as a result, to a macroscopic lubricating effect [17,18].

Although the TMDs give the PVD coatings a self-lubricating character, they cannot withstand high tribological loads in cold forging process with high contact pressures up to $\sigma_c = 2{,}500$ MPa [19]. This attributes to their mechanical weakness and low wear resistance, e.g. low universal hardness $HU \leq 10$ GPa [7]. Therefore, TMDs within the coating must be incorporated into a hard matrix, in order to increase the wear resistance of the forming tools in contact with workpieces. The ternary chromium based nitride coating systems are promising candidates for this purpose. (Cr,Al)N coatings deposited by physical vapor deposition are widely reported exhibiting high hardness, good abrasion wear resistance and high corrosion resistance [20-30]. Direct current magnetron sputtering (dcMS) or high power pulse magnetron sputtering (HPPMS) are among the deposition technologies for synthesis of (Cr,Al)N. By means of dcMS technology, higher deposition rates compared to the HPPMS can be achieved [31, 32]. On the other hand, the HPPMS technology generally operates at short pulse lengths of several tens of microseconds [22-25, 33, 34] and with frequencies $10\ \text{Hz} \leq f_{pulse} \leq 10\ \text{kHz}$ [22, 25, 33-36]. Therefore, HPPMS provides high peak current and high ionization degree, which are much higher than those of conventional dcMS. This leads to higher plasma densities using HPPMS, which results in deposition of dense coatings with high values of universal hardness HU and indentation modulus E_{IT} [24, 37-41]. Another advantage of HPPMS compared with dcMS is the higher capability for coating of complex-shaped tools with surfaces not facing the target, e.g. the tools applied in the cold forging of steel [23, 42]. A hybrid process consisting of dcMS and HPPMS combines the advantages of both technologies. The main focus of this paper is therefore to use the hybrid technology dcMS/HPPMS for the deposition of a coating system on complex shaped tools, which combines the advantages of the $(Cr_{1-x}Al_x)N$ and MoS_y constituents, as well as tribological investigations by means of model tests. A further objective of this study is the understanding of the influence of nitrogen content of the coating on the mechanical and tribological behavior of the substrate/coating compound under the condition of dry cold forging.

2 Experimental procedure

2.1 Deposition process of the $(Cr_{1-x}Al_x)N+MoS_y$ coating

The investigated coatings were deposited on tool steel substrates of X155CrMoV12 (DIN 1.2379, AISI D2), with chemical composition of $x_C = 1.55$, $x_{Si} = 0.33$, $x_{Mn} = 0.34$, $x_P = 0.02$, $x_S = 0.008$, $x_{Cr} = 11.94$, $x_{Mo} = 0.72$ and $x_W = 1.00$. This steel belongs to the typical tool materials in cold forging [43]. The substrates were hardened to a hardness of (60 ± 1) HRC. The steel specimens were prepared with a diameter $Ø_{sub} = 26$ mm and a thickness $d = 8$ mm and polished to an arithmetic mean roughness of $Ra = 0.02$ µm. In order to investigate the distribution of coating thickness along the length of forging tools, an experimental tool with the same aspect ratio as the forging tools was designed. Four cemented carbide WC substrates THM12, Kennametal Widia Produktions GmbH & Co. KG, Essen, Germany, were fixed at specific positions along the longitudinal axis of the experimental tool, namely positions P1 to P4. Figure 1 schematically shows a side view of the experimental tool. The die shoulder at position P2 had an angle of $\alpha = 45°$. The front and back sides of each THM12 substrate are denoted in Figure 1 with P_F and P_B, i.e. P_{1F} indicates the front and P_{1B} the back side of sample in position P1, in relation to the direction of the workpiece motion.

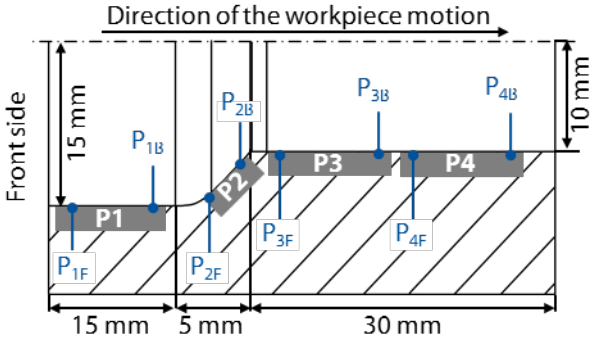

Figure 1: Schematic of the experimental tool and the THM12 substrates at positions 1 to 4

The substrates at the positions P1, P3 and P4 were prepared with a length $L = 12.7$ mm, a width $W = 12.7$ mm and a height $H = 4.76$ mm. The specimen at position P2 had a comparably shorter length $L = 6.0$ mm. The investigated coatings were deposited using a hybrid dcMS/HPPMS process in an industrial scale coating unit CC800/9 Custom, CemeCon AG, Wuerselen, Germany. The coating unit is equipped with two HPPMS and four dcMS power supplies. The coating setup and the positioning of the experimental tool are schematically shown in Figure 2.

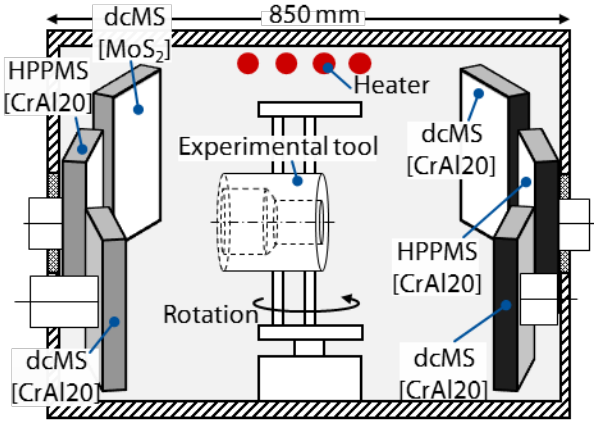

Figure 2: Schematic of coating deposition setup

During deposition, the samples were moved in a one-fold rotation. The substrates were mounted using a sample holder, which was positioned parallel to the cathodes. One MoS_2 and five plugged CrAl20 targets were used for the deposition of $(Cr_{1-x}Al_x)N+MoS_y$ coatings. Each of the twenty Al plugs within the CrAl20 target has a diameter of $Ø$ = 15 mm. Each of the targets has a length L = 500 mm and a width W = 80 mm. The MoS_2 target has a purity of w_{MoS_2} = 99.5 wt. %. The purities of chromium and aluminum in CrAl20 targets are w_{Cr} = 99.9 wt. % and w_{Al} = 99.5 wt. %, respectively. The MoS_2 target was mounted on one of the four dcMS power supplies. The other three dcMS and two HPPMS cathodes were equipped with CrAl20 targets.

In order to investigate the influence of nitrogen content of the coating on the mechanical and tribological behavior of the substrate/coating compound under the condition of dry cold forging, two coating systems with different nitrogen contents were deposited. For this purpose, argon and nitrogen were used as process and reactive gases. Pressure of the coating unit was controlled to remain p = 660 mPa in the first and p = 710 mPa in the second process by adjusting the concentration of N_2. This led to two nitrogen fluxes $F(N_2)$ = 157 sccm and $F(N_2)$ = 175 sccm into the coating chamber. The two coating systems $(Cr_{1-x}Al_x)N+MoS_y$ deposited with $F(N_2)$ = 157 sccm and $F(N_2)$ = 175 sccm will be termed in the following as S_{N157} and S_{N175}, respectively. The coatings S_{N157} and S_{N175} were bonded to the substrates using a (Cr,Al)-bond coat. An interlayer (Cr,Al)N was thereafter deposited on the top of (Cr,Al)-bond coat to increase the adhesion between the substrate and the coating system $(Cr_{1-x}Al_x)N+MoS_y$. A deposition time of t = 47 min was used for all coatings. The process parameters for deposition of coatings S_{N157} and S_{N175} are listed in Table 1.

Table 1: Process parameters for deposition of coating system $(Cr_{1-x}Al_x)N+MoS_y$

Process parameter	Unit	Value
Max. substrate temperature, T	°C	480
Pressure, p	mPa	660/710
Argon flux, $F(Ar)$	sccm	200
Nitrogen flux, $F(N_2)$ (pressure controlled)	sccm	157/175
dcMS cathode power, $P_{dcMS\text{-}MoS_2}$	kW	2
dcMS cathode power, $P_{dcMS\text{-}CrAl20}$	kW	3
HPPMS mean cathode power, $P_{HPPMS\text{-}CrAl20}$	kW	5
Pulse frequency, f_{pulse}	Hz	500
Pulse length, t_{on}	µs	40
Bias voltage (dc), U_{bias}	V	-100

2.2 Analysis methods for the coating properties

In order to evaluate the morphology and thickness of the coatings, micrographs of fractured cross sections were taken using secondary electrons (SE) detector in a scanning electron microscope (SEM) ZEISS DSM 982 Gemini, Carl Zeiss AG, Oberkochen, Germany. Measurements of surface roughness were performed according to ISO 4287 using a confocal laser scanning microscope (CLSM) Keyence VK-X210, Tokio, Japan. For each coating 30 measurements were carried out and an average of results was considered as arithmetic average roughness Ra of the coating. The chemical composition of the coatings was determined by using glow discharge optical emission spectroscopy (GDOES) in radio frequency (rf) mode. A GDOES profiler type JY 5000 RF, HORIBA Jobin Yvon Ltd., Kyoto, Japan, was used. A Nanoindenter of type TI 950 TriboIndenter, Bruker Corporation, Billerica, Massachusetts, USA, with a Berkovich indenter was applied for the determination of the mechanical properties universal hardness HU and indentation modulus E_{IT}. The penetration depth was kept below 10 % of the top layer thickness. Calculations of the modulus of indentation are based on Oliver and Pharr's equations [44]. A constant Poisson's ratio of υ = 0.25 was assumed for the coatings according to [12].

2.3 Investigation of the compound properties

Adhesion strength of the investigated substrate/coating compounds were evaluated using the conventional methods Rockwell indentation and scratch test. A diamond cone Brale indenter with a tip radius of r = 200 µm and a cone angle of θ = 120° was applied for the measurements. Rockwell (HRC) indentation tests were performed according to DIN EN ISO 6508 with a load F = 1,471 N, followed by analyses of residual indents by means of CLSM. The evaluation of the adhesion strength between substrate and coating was preceded according to currently withdrawn VDI guideline 3198 by distinguishing between different adhesion classes HF from HF1 to HF6. In this regard, HF1 represents an excellent adhesion and HF 5 and HF6, indicate an insufficient adhesion. A quantitative analysis of adhesion of substrate/coating compounds was achieved by scratch testing according to DIN EN 1071-3 (ISO 20502). In this regard, the scratches were performed at different loads and the adhesion between substrate and coating was quantified through determination of the critical loads L_{C1} - L_{C3}.

2.4 Investigations of tribological behavior

The tribological tests were conducted in a pin-on-disc (PoD) tribometer, CSM instruments SA, A company of Anton Paar, Peseux, Switzerland, in order to simulate tribological behavior during dry cold forging. Pins of 16MnCr5 (DIN 1.7131, AISI 5115) with a diameter of $Ø_{pin}$ = 6 mm were chosen as counterparts. 1.7131 is one of the typical semi-finished products in cold forging [43]. Pins were pressed in off-center position onto the uncoated reference specimen and the coated samples with a track radius of r = 5.0 mm. The applied constant normal load in PoD tests was calculated on the basis of the Hertzian

pressure concept sphere on flat plate. Here, the Hertzian pressure can be determined using the constant normal load, diameter of the pin as well as the material properties of the pins and specimens. Based on the calculation results, a constant normal load of F_N = 10 N, corresponding to a maximum Hertzian pressure of $\sigma \approx 2{,}000$ MPa was chosen for the PoD tests, which is in agreement with the contact pressures existing in the cold forging of steel [19]. The tests were performed at room temperature T = 23 °C, under controlled air atmosphere with a relative humidity of RH = (32 ± 2) %. Relative velocity was v = 5 cm/s, corresponding to the usual velocity in dry full forward extrusion. Tribological investigations were carried out for a sliding distance of l = 200 m. Tribo-chemical film formation onto the wear tracks and their counterparts were examined by means of a mico-Raman spectrometry, inVia REFLEX, RENISHAW, Gloucestershire, United Kingdom. A laser with excitation wavelength λ = 532 nm with laser intensities 1 % and 10 % was used. The laser exposure time was t = 20 s. The comparatively low laser intensity ensures that no chemical modification of the tribo-chemical films and coatings occurs. Before each measurement, a calibration was performed using reference silicon sample with a known Raman shift of $\tilde{\upsilon}$ = 520 cm^{-1}. The measurements on each location were examined three times. The Raman spectra 200 cm^{-1} ≤ $\tilde{\upsilon}$ ≤ 2,000 cm^{-1} was acquired from the center of the worn tracks on tribo-chemical films.

3 Results and discussion

3.1 Coating properties

Figure 3 shows SEM cross section fractures of the $(Cr_{1-x}Al_x)N+MoS_y$ coatings S_{N157} (Figure 3(a)) and S_{N175} (Figure 3(b)). The coating S_{N157} has a thickness of s = 1.75 µm and thickness of S_{N175} is s = 1.68 µm.

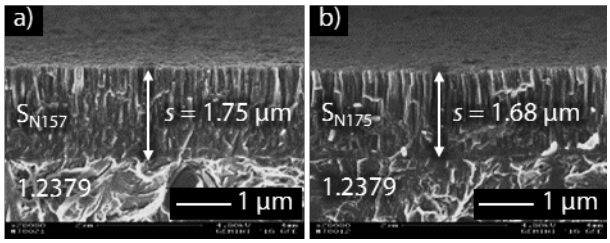

Figure 3: SEM cross section fractures of the S_{N157} (a) and S_{N175} (b) coated 1.2379 substrates

Based on the SEM analyses both, the S_{N157} and S_{N175} coatings exhibit a fine and columnar morphology. By means of CLSM investigations, an arithmetic average surface roughness Ra = 0.02 µm was determined for the coatings S_{N157} and S_{N175}. Table 2 shows the chemical composition of the deposited coatings as measured by GDOES. A decrease in the chromium content of $\Delta x_{Cr} \approx 7$ at.% and an increase in the nitrogen content of $\Delta x_{Cr} \approx 7$ at.% occurs from sample S_{N157} to S_{N175}. The possible reason for the decrease in chromium content of the coating with increasing the nitrogen partial pressure is the stronger poisoning of the chromium area within the plugged CrAl20 target compared to the Al plugs. This subject will be more studied in our future works, where comprehensive investigations on crystal structure and elemental composition of the coating systems will be also performed by means of transmission electron microscopy (TEM) and X-ray photoelectron spectroscopy (XPS).

Table 2: Chemical composition of the $(Cr_{1-x}Al_x)N+MoS_y$ coatings S_{N157} and S_{N175}

Element	S_{N157} [at.%]	S_{N175} [at.%]
Al	8.5	8.5
Cr	49.3	42.2
N	33.4	40.5
S	0.7	0.9
Mo	8.1	8.0

The results of chemical analyses reveals comparable values of ratio [(Mo+S)/(Cr,Al)N] of samples S_{N157} and S_{N175}. Both coatings have a [(Mo+S)/(Cr,Al)N] = 6.1 %. The mechanical properties universal hardness HU and indentation modulus E_{IT} of the coatings S_{N157} and S_{N175} were determined using nanoindentation and are given in Table 3.

Table 3: Mechanical properties of the $(Cr_{1-x}Al_x)N+MoS_y$ coatings S_{N157} and S_{N175}

	S_{N157}	S_{N175}
Universal hardness HU [GPa]	18.0 ± 3.4	18.5 ± 2.7
Indentation Modulus E_{IT} [GPa]	330.1 ± 21.3	362.7 ± 46.7

The coatings S_{N157} and S_{N175} do not show extreme differences in the values of universal hardness. However, the sample S_{N157} with a lower nitrogen content has a lower indentation modulus of E_{IT} = (330.1 ± 21.3) GPa compared to the coating S_{N175} with E_{IT} = (362.7 ± 46.7) GPa.

For the investigations on the coating thickness distribution along the longitudinal axis of the forging tool, the coated THM 12 substrates positioned at P1 to P4 of the experimental tool were considered. The front and back side of each sample were subsequently analyzed by mean of SEM. Since the both coating systems exhibited similar trend regarding the thickness distribution at positions P1 to P4, only the corresponding results to the coating system S_{N175} will be presented in this paper. Figure 4(a-h) shows the SEM cross section fractures of S_{N175} coated substrates at positions P_{1F} to P_{4B}. Additionally, the surface roughness Ra of each position is given in Figure 4(a-h).

The SEM images in Figure 4(a-h) indicate that the entire length of the experimental tool is coated. Furthermore, the morphology of the coating differs slightly with respect to the distance from the targets in

coating unit. In this regard, the sample located in the front side of the experimental tool at position P1 reveals the maximum deviation from a vertical orientation of coating's columns, which will be generally observed for the samples located parallel to the targets in coating unit (Figure 3). The microstructural coating's columns at P1 exhibit an orientation of $\theta = 50°$ (Figure 4(a) and (b)). By a change in the orientation of substrate's surface with respect to the targets, the coating at P_{2F} and P_{2B} exhibits a fine and dense morphology (Figure 4(c) and (d)). Within the position P3, the morphology changes again to a columnar microstructure. However, the inclination of the columns approaches gradually to $\theta = 90°$ along the longitudinal axis of the experimental tool. The orientation of microstructural columns in S_{N175} changes from $\theta = 54°$ at P_{3F} to $\theta = 71°$ at P_{3B} and reaches $\theta = 90°$ at P_{4F}. At position P_{4B}, some portions of the sputtered atoms enter the experimental tool from the back side and precipitate additionally onto the substrate. This extra coating resource lead to reversely inclined columns at P_{4B} with respect to the vertical direction and an orientation of $\theta = 115°$.

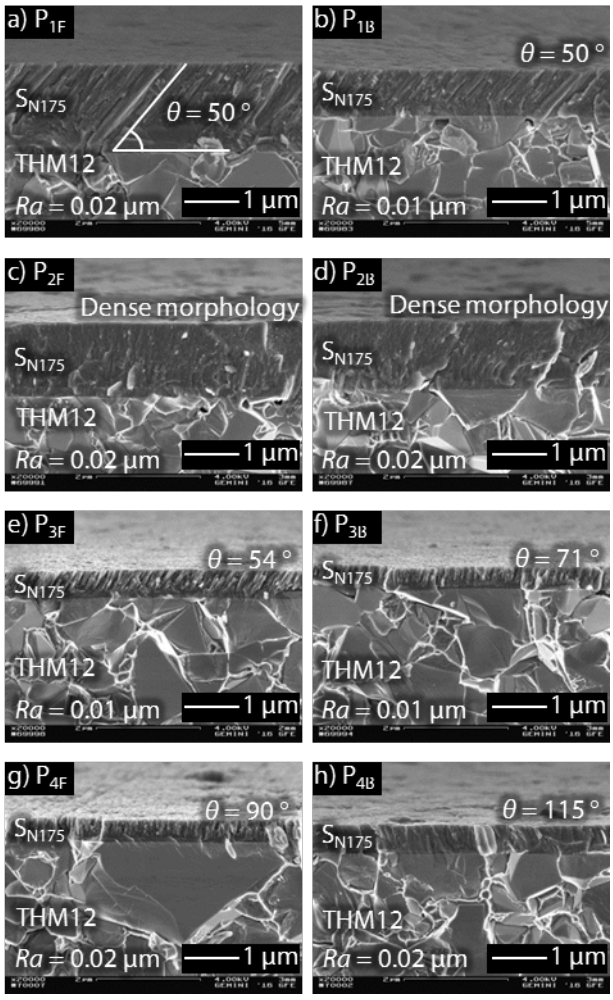

Figure 4: SEM cross section images of the S_{N175} coated THM12 substrates positioned at P_{1F} to P_{4B} (a-h) along the longitudinal axis of the experimental tool and the corresponding values of *Ra*

Another result of deposition from both, the front and back side of the experimental tool, is a slightly higher coating thickness at P_{4B} compared to P_{4F}. For the comparison reasons, the distribution of the coating thickness along the longitudinal axis of the experimental tool is presented in Figure 5 with respect to the positions P_{1F} to P_{4B}.

It is observed, that the coating thickness gradually decreases along the longitudinal axis of the experimental tool, except at the die shoulder and at the end of the experimental tool. The die shoulder has an angle of $\alpha = 45°$ and is in a higher degree of line-of-sight of the plasma source in comparison with the other positions along the longitudinal axis of the experimental tool with a perpendicular orientation with respect to the targets in the coating unit. This leads to an increase in the coating thickness. After the die shoulder, again the coating thickness decreases gradually, until the positions near the back side of the experimental tool. Here, the substrate receives the coating's ingredients from both, the front and back side of the experimental tool, which results in a slightly higher coating thickness at P_{4B} in comparison with P_{4F}.

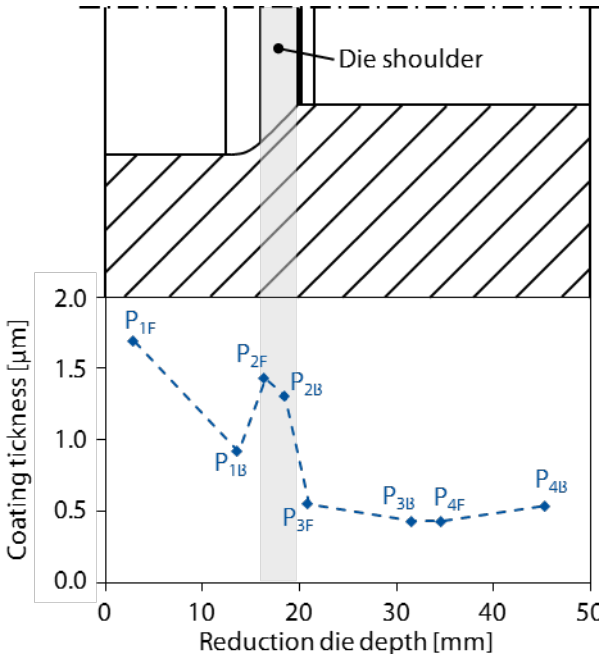

Figure 5: Thickness distribution of the coating S_{N175} along the longitudinal axis of the experimental tool

3.2 Compound properties

The adhesion between the steel substrate 1.2379 and the coatings S_{N157} and S_{N175} was studied using the conventional methods Rockwell indentation and scratch test. Figure 6(a) and Figure 6(b) show the CLSM images of Rockwell indents on both compounds.

The results of Rockwell indentation tests on the compounds 1.2379/S_{N157} and 1.2379/S_{N175} reveal fine cracks at the imprint edges. However, neither spalling nor adhesive failures of S_{N157} and S_{N175} on 1.2379 occurs. Thus, the compounds 1.2379/S_{N157} and

1.2379/S_{N175} are assigned the adhesion class HF 1, in accordance with VDI guideline 3198.

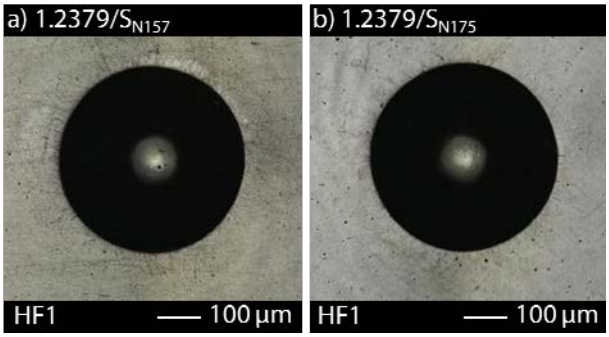

Figure 6: CLSM micrographs of Rockwell indents on 1.2379/S_{N157} (a) and 1.2379/S_{N175} (b) for determination of adhesion classes (HF)

In addition to the Rockwell indentation tests, adhesion strength of compounds was quantitatively investigated by means of scratch tests. For this purpose, different constant loads were applied and the resulted scratch tracks were analyzed using CLSM. In this work, only the results of critical loads L_{C1} to L_{C3} will be discussed. The CLSM images of scratch tracks on compounds 1.2379/S_{N157} and 1.2379/S_{N175} corresponding to L_{C1} to L_{C3} are given in Figure 6(a-c) and Figure 6(d-f), respectively.

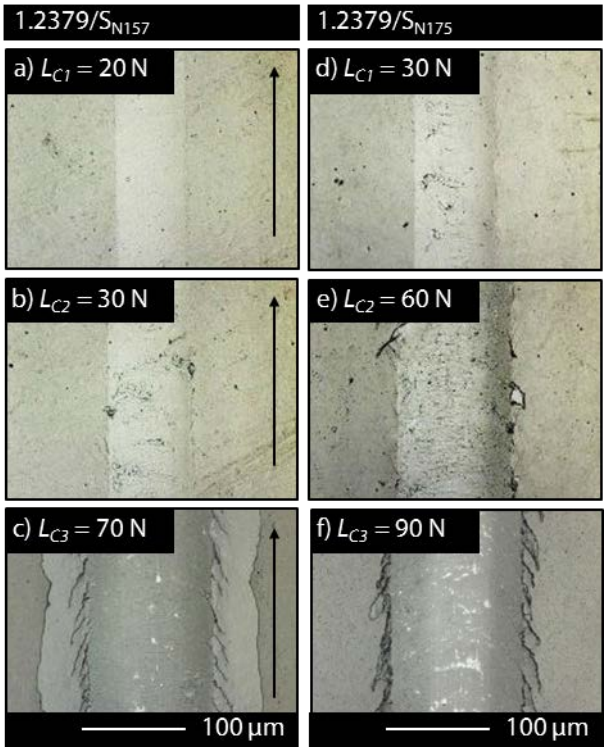

Figure 6: CLSM micrographs of scratch tracks on 1.2379/S_{N157} (a-c) and 1.2379/S_{N175} (d-f) after scratch tests with critical loads L_{C1}, L_{C2} and L_{C3}

The CLSM analyses of 1.2379/S_{N157} show a low plastic deformation after scratch test with a constant critical load L_{C1} = 20 N (Figure 6(a)). However, a high adhesion strength between the substrate and S_{N157} in scratch tests was observed up to L_{C2} = 30 N. At this load, slight spalling of the coating at the scratch edges can be detected (Figure 6(b)). The onset of this damage regime is represented with L_{C2} = 30 N, in accordance with DIN EN 1071-3. By increasing the scratch load to L_{C3} = 70 N an adhesive failure of S_{N157} in the compound 1.2379/S_{N157} occurs (Figure 6(c)). For the compound 1.2379/S_{N175}, a higher adhesion between substrate and coating was observed. A slight plastic deformation of 1.2379/S_{N175} occurs after scratch test with L_{C1} = 30 N in Figure 6(d). Furthermore, small scales cohesive failures of the coating can be detected on the scratch track at L_{C2} = 60 N. These are observable as irregular chippings of the coating through the scratch track in Figure 6(e). However, this damage regime did not change considerably by increasing the scratch load. A scratch load of L_{C3} = 90 N leads to spalling and chipping of the coating from the substrate through the scratch track. Based on results of scratch tests, the compound 1.2379/S_{N175} exhibits higher adhesion strength between substrate and coating compared to 1.2379/S_{N157}. Analyses of the coating and compound properties of the samples P1 to P4 is the subject of our current studies.

3.3 System properties

For the investigations on friction behavior of the coated samples, model tests under dry sliding conditions were performed using the PoD tribometer. Additionally, the uncoated steel 1.2379 was analyzed as reference in PoD tests, in order to compare the results with the S_{N157} and S_{N175} coated substrates. Figure 7 shows the CoF of the uncoated substrate 1.2379 as well as the compounds 1.2379/S_{N157} and 1.2379/S_{N175} against 1.7131 counterpart pin.

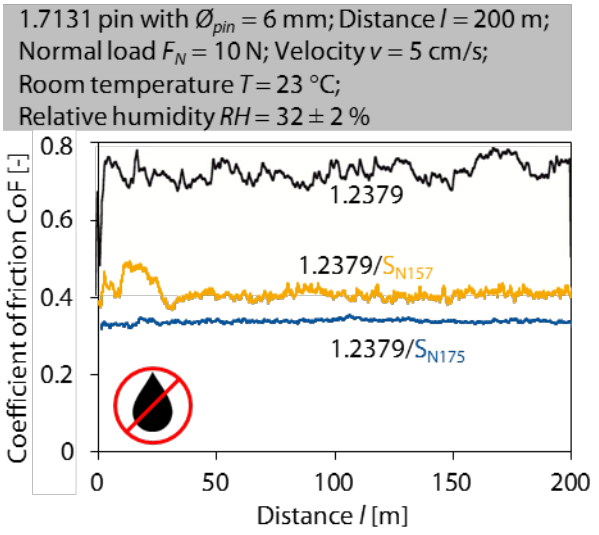

Figure 7: Coefficient of friction of the uncoated 1.2379 substrate and coated samples 1.2379/S_{N157} and 1.2379/S_{N175} against 1.7131 using PoD tribometer

Based on the results of PoD tests, both coated samples 1.2379/S_{N157} and 1.2379/S_{N175} exhibit lower CoF compared to the uncoated substrate. Furthermore, the lowest value of CoF = 0.34 is achieved with the compound 1.2379/S_{N175}. Under the same condition, the compound 1.2379/S_{N157} has a CoF = 0.42, whereas the uncoated substrate 1.2379 shows the highest coefficient of friction CoF = 0.75.

In order to explain the observed friction behavior under PoD tests, the contact areas in all samples were analyzed by means of Raman spectroscopy. For this purpose, the worn tracks on uncoated 1.2379 and the compounds 1.2379/S_{N157} and 1.2379/S_{N175} were examined regarding the formation of tribo-chemical films. The corresponding 1.7131 counterpart pins were also analysed using Raman spectroscopy. Additionally, unworn coated samples as deposited were investigated as references in order to ensure, that no reaction films were formed before the PoD tests. The Raman spectra of the formed films on the investigated tribologial systems and the unworn compounds are shown in Figure 8.

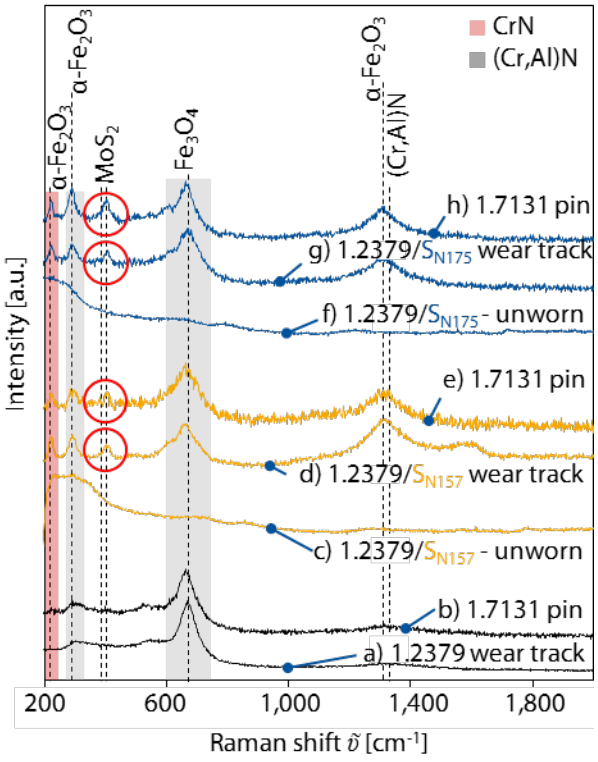

Figure 8: Raman spectra of the uncoated 1.2379 substrate, S_{N157} and S_{N175} coated samples and counterparts after PoD model tests as well as spectra of as deposited samples

In the Raman spectra, the peaks at $\tilde{\upsilon}$ = 220 cm^{-1}, $\tilde{\upsilon}$ = 290 cm^{-1} and $\tilde{\upsilon}$ = 1,310 cm^{-1} correspond to the formation of the iron oxide hematite α-Fe_2O_3 [45]. The origin of Raman peaks at $\tilde{\upsilon}$ = 677 cm^{-1} is attributed to the formation of Fe_3O_4 [46]. The two bands centred at $\tilde{\upsilon}$ = 296 cm^{-1} and $\tilde{\upsilon}$ = 640 cm^{-1} and the peak at $\tilde{\upsilon}$ = 1,356 cm^{-1} correspond to (Cr,Al)N [21, 47]. Furthermore, the band centered at $\tilde{\upsilon}$ = 238 cm^{-1} indicates the formation of CrN [48]. The Raman spectroscopy analyses on uncoated 1.2379 (Figure 8(a)) and the counterpart pin (Figure 8(b)) show the existence of α-Fe_2O_3 and Fe_3O_4. The formation of these iron oxides can be recognized for all other tribological systems, except the unworn specimens 1.2379/S_{N157} (Figure 8(c)) and 1.2379/S_{N175} (Figure 8(f)). However, a precise statement about the formation of α-Fe_2O_3 and Fe_3O_4 on the compounds and pins cannot be provided, due to the vicinity of their corresponding peaks to those of CrN and (Cr,Al)N. Besides the mentioned peaks, both the compounds and their corresponding pins reveal one further peak centered at 383 cm^{-1} ≤ $\tilde{\upsilon}$ ≤ 408 cm^{-1}. This is particularly observable for the tribological system, consisting of the 1.2379/S_{N175} (Figure 8(g)) and the pin (Figure 8(h)). These peaks attributes to the formation of self-lubricating film MoS_2 [49-51]. Such peaks cannot be detected for the uncoated steel (Figure 8(a)) and unworn area of the investigated compounds (Figure 8(c) and (f)). This confirms a formation of MoS_2 during the tribological tests, which can be attributed to the contact pressures. A more formation of self-lubricating film MoS_2 on the compound and counterpart during the tribological loading leads to the lower CoF of 1.2379/S_{N175} compared to the 1.2379/S_{N157} and uncoated substrate. Based on the results, the investigated self-lubricating coating system ($Cr_{1-x}Al_x$)N+MoS_y exhibits a high potential for lubricant-free “green” cold forging of steel.

4 Conclusion and outlook

Within the scope of this paper, two coating systems ($Cr_{1-x}Al_x$)N+MoS_y with two different nitrogen contents were deposited on tool steel 1.2379. For the coating deposition an industrial hybrid technology, consisting of dcMS/HPPMS was applied. In order to investigate the coating thickness distribution along the longitudinal axis of the complex-shaped forging tools, an experimental tool was designed and coated. After characterization of the coating and compound properties, samples were investigated regarding their tribological behavior. For this purpose, application oriented wear tests on uncoated and coated samples were performed by means of a PoD tribometer. The PoD tests were conducted using pins made of 1.7131 under dry conditions and included the determination of coefficients of friction. Based on the results, the coated samples exhibit lower coefficients of friction than uncoated 1.2379. Furthermore, the coated sample with higher nitrogen content reveals better tribological properties. Using the Raman investigations it can be concluded that this phenomenon is due to the formation of self-lubricating MoS_2 films on the surface of sample and counterpart under the tribological loads. Therefore, the investigated coating system ($Cr_{1-x}Al_x$)N+MoS_y exhibits a high potential for lubricant-free “green” cold forging of steel. In future works, more comprehensive investigations on crystal structure and elemental composition of the coating systems will be performed using TEM and XPS, in order to explain the influence of nitrogen content on the tribological behavior of coated specimens in contact with 1.7131.

Acknowledgements

The research was funded by the German Research Foundation (Deutsche Forschungsgemeinschaft DFG) within the priority program „Dry metal forming – sustainable production through dry processing in metal forming (Trockenumformen – Nachhaltige Produktion durch Trockenbearbeitung in der Umformtechnik (SPP 1676).

References

[1] F. Klocke: Manufacturing processes 4 - Forming, Springer, (2013).

[2] F. Klocke, T. Maßmann, K. Bobzin, E. Lugscheider, N. Bagcivan, Carbon based tool coatings as an approach for environmentally friendly metal forming processes, Wear 260 (2006) 287–295.

[3] F. Klocke, T. Maßmann, K. Gerschwiler, Combination of PVD tool coatings and biodegradable lubricants in metal forming and machining, Wear 259 (2005) 1197–1206.

[4] K. Bobzin, N. Bagcivan, P. Immich, C. Warnke, F. Klocke, C. Zeppenfeld, P. Mattfeld, dvancement of a nanolaminated TiHfN/CrN PVD tool coating by a nano-structured CrN top layer in interaction with a biodegradable lubricant for green metal forming, Surface and Coatings Technology 203 (2009) 3184–3188.

[5] E. Lugscheider, K. Bobzin, C. Piñero, F. Klocke, T. Massmann, Development of a superlattice (Ti,Hf,Cr)N coating for cold metal forming applications, Surface and Coatings Technology 177-178 (2004) 616–622.

[6] F. Vollertsen, F. Schmidt: Dry Metal Forming: Definition, Chances and Challenges. Int. J. Precision Engineering and Manufacturing – Green Technology 1/1 (2014) 59–62.

[7] T. Mang (Ed.), Lubricants and lubrication, 2., completely rev. and extended ed. ed., Wiley-VCH, Weinheim (2007).

[8] C. Donnet, A. Erdemir, Solid lubricant coatings: recent developments and future trends, Tribology Letters 17 (2004) 389–397.

[9] P. Mutafov, M. Evaristo, A. Cavaleiro, T. Polcar, Structure, mechanical and tribological properties of self-lubricant W–S–N coatings, Surface and Coatings Technology 261 (2015) 7–14.

[10] C. Donnet, J.M. Martin, T. Le Mogne, M. Belin, Super-low friction of MoS_2 coatings in various environments, Tribology International 29 (1996) 123–128.

[11] A. Aubert, J. Nabot, J. Ernoult, P. Renaux, Preparation and properties of MoS_x films grown by d.c. magnetron sputtering, Surface and Coatings Technology 41 (1990) 127–134.

[12] K. Bobzin, T. Brögelmann, N.C. Kruppe, S. Bastürk, F. Klocke, P. Mattfeld, D. Trauth, Tribological Behavior of $(Cr_{1-x}Al_x)N/WS_y$ PVD Tool Coatings for the Application in Dry Cold Forging of Steel, Dry Metal Forming Open Access Journal 1 (2015) 152–158.

[13] F. Klocke, D. Trauth, P. Mattfeld, A. Shirobokov, K. Bobzin, T. Brögelmann, S. Bastürk, Multiscale FE-Studies of Contact Stresses of Dry and Lubricated Shot Peened Workpiece Surfaces, Dry Metal Forming Open Access Journal 1 (2015) 11–16.

[14] F. Klocke, D. Trauth, R. Hild, P. Mattfeld, K. Bobzin, S. Bastürk, T. Brögelmann, Numerical Analysis of the Tribological Mode of Action in Cold Forming of Sinus Waved Surfaces Structures, Dry Metal Forming Open Access Journal 1 (2015) 137-142.

[15] K. Bobzin, T. Brögelmann, S. Bastürk, F. Klocke, P. Mattfeld, D. Trauth, P. Polcik, S. Kolozsvari, Influence of the Composition on the Properties of $(Cr_{1-x}Al_x)N/Mo_yS_z$ PVD Coatings, Advanced Engineering Materials 18 (2016) 1036-1043

[16] K. Bobzin, T. Brögelmann, R. H. Brugnara, N. C. Kruppe, S. Bastürk, F. Klocke, P. Mattfeld, R. Hild, D. Trauth, Influence of the Chemical Composition on the Properties of HPPMS $(Cr_{1-x},Al_x)N/WS_y$ Coatings for the Application on Dry Cold Forging Processes, 12th International Conference THe "A" Coatings 2016, Hannover, Germany (2016).

[17] K. Bobzin, E. Lugscheider, R. Nickel, N. Bagcivan, A. Krämer, Wear behavior of $Cr_{1-x}Al_xN$ PVD-coatings in dry running conditions, Wear 263 (2007) 1274–1280.

[18] J.-F. Yang, B. Parakash, J. Hardell, Q.-F. Fang, Tribological properties of transition metal di-chalcogenide based lubricant coatings, Frontiers of Materials Science 6 (2012) 116–127.

[19] N. Bay, A. Azushima, P. Groche, I. Ishibashi, M. Merklein, M. Morishita, T. Nakamura, S. Schmid, M. Yoshida, Environmentally benign tribosystems for metal forming, CIRP Annals - Manufacturing Technology 59 (2010) 760–780.

[20] K. Bobzin, T. Brögelmann, N.C. Kruppe, M. Arghavani, S. Bastürk, F. Klocke, P. Mattfeld, D. Trauth, R. Hild, HPPMS $(Cr_{1-x}Al_x)N+WS_y$ Coatings for the Application in Dry Cold Forging of Steel: Synthesis and Raman Characterization, Dry Metal Forming Open Access Journal 2 (2016) 72-77.

[21] K. Bobzin, T. Brögelmann, N.C. Kruppe, S. Bastürk, F. Klocke, P. Mattfeld, D. Trauth, R. Hild, Synthesis, characterization, and tribological evaluation of $(Cr_{1-x}Al_x)N+MoS_y$ coatings, Surface and Coatings Technology 308 (2016) 383–393.

[22] N. Bagcivan, K. Bobzin, S. Theiß, Synthesis of nanostructured HPPMS CrN/AlN coatings, Journal of Physics D: Applied Physics 46 (2013) 84001.

[23] N. Bagcivan, K. Bobzin, S. Theiß, $(Cr_{1-x}Al_x)N$: A comparison of direct current, middle frequency pulsed and high power pulsed magnetron sputtering for injection molding components, Thin Solid Films 528 (2013) 180–186.

[24] K. Bobzin, N. Bagcivan, P. Immich, S. Bolz, R. Cremer, T. Leyendecker, Mechanical properties and oxidation behaviour of (Al,Cr)N and (Al,Cr,Si)N coatings for cutting tools deposited by HPPMS, Thin Solid Films 517 (2008) 1251–1256.

[25] N. Bagcivan, K. Bobzin, A. Ludwig, D. Grochla, R.H. Brugnara, CrN/AlN nanolaminate coatings deposited via high power pulsed and middle frequency pulsed magnetron sputtering, Thin Solid Films 572 (2014) 153–160.

[26] X.-z. Ding, A. Tan, X.T. Zeng, C. Wang, T. Yue, C.Q. Sun, Corrosion resistance of CrAlN and TiAlN coatings deposited by lateral rotating cathode arc, Thin Solid Films 516 (2008) 5716–5720.

[27] N. Bagcivan, K. Bobzin, T. Brögelmann, C. Kalscheuer, Development of (Cr,Al)ON coatings using middle frequency magnetron sputtering and investigations on tribological behavior against polymers, Surface and Coatings Technology 260 (2014) 347–361.

[28] B.S. Kim, G.S. Kim, S.Y. Lee, B.Y. Lee, Effects of Al target power on the mechanical and oxidation resistance of the CrN/AlN multilayer coatings, Surface and Coatings Technology 202 (2008) 5526–5529.

[29] K. Bobzin, T. Brögelmann, R.H. Brugnara, M. Arghavani, T.-S. Yang, Y.-Y. Chang, S.-Y. Chang, Investigation on plastic behavior of HPPMS CrN, AlN and CrN/AlN-multilayer coatings using finite element simulation and nanoindentation, Surface and Coatings Technology 284 (2015) 310–317.

[30] K. Bobzin, T. Brögelmann, N.C. Kruppe, M. Arghavani, J. Mayer, T.E. Weirich, On the plastic deformation of chromium-based nitride hard coatings deposited by hybrid dcMS/HPPMS: A fundamental study using nanoscratch test, Surface and Coatings Technology 308 (2016) 298–306.

[31] J. Čapek, M. Hála, O. Zabeida, J. E. Klemberg-Sapieha, L. Martinu, Deposition rate enhancement in HiPIMS without compromising the ionized fraction of the deposition flux, Journal of Physics D: Applied Physics 46 (2013) 205205.

[32] M. Samuelsson, D. Lundin, J. Jensen, M. A. Raadu, J. T. Gudmundsson, U. Helmersson, On the film density using high power impulse magnetron sputtering, Surface and Coatings Technology 205 (2010) 591-596.

[33] K. Bobzin, T. Brögelmann, R. H. Brugnara, Aluminum-rich HPPMS $(Cr_{1-x},Al_x)N$ coatings deposited with different target compositions and at various pulse lengths, Vacuum 122 (2015) 201-27.

[34] K. Sarakinos, J. Alami, S. Konstantinidis, High power pulsed magnetron sputtering: A review on scientific and engineering state of the art, Surface and Coatings Technology 204 (2010) 1661-1684.

[35] K. Bobzin, T. Brögelmann, R. H. Brugnara, N. C. Kruppe, S. Chromy, Influence of HPPMS pulse parameters on the reactive gas N_2 and on the properties of (Cr, Al)N coatings, Surface and Coatings Technology 293 (2016) 28-34.

[36] D. Lundin, K. Sarakinos, An introduction to thin film processing using high-power impulse magnetron sputtering, Journal of Materials Research 27 (2012) 780-792.

[37] N. Bagcivan, K. Bobzin, G. Grundmeier, M. Wiesing, O. Ozcan, C. Kunze, R. H. Brugnara, Influence of HPPMS pulse length and inert gas mixture on the properties of (Cr,Al)N coatings, Thin Solid Films 549 (2013) 192-198.

[38] J. Lin, W. D. Sproul, J. J. Moore, S. Lee, S. Myers, High rate deposition of thick CrN and Cr_2N coatings using modulated pulse power (MPP) magnetron sputtering, Surface and Coatings Technology 205 (2011) 3226-3234.

[39] J. Alami, P. O. Å. Persson, D. Music, J. T. Gudmundsson, J. Bohlmark, U. Helmersson, Ion-assisted physical vapor

deposition for enhanced film properties on nonflat surfaces, J. Vac. Sci. Technol. A 23 (2005) 278-280.
[40] M. Lattemann, A. P. Ehiasarian, J. Bohlmark, P. O. Å. Persson, U. Helmersson, Investigation of high power impulse magnetron sputtering pretreated interfaces for adhesion enhancement of hard coatings on steel, Surface and Coatings Technology 200 (2006) 6495-6499.
[41] J. Lin, J. J. Moore, W. D. Sproul, B. Mishra, Z. Wu, J. Wang, The structure and properties of chromium nitride coatings deposited using dc, pulsed dc and modulated pulse power magnetron sputtering, Surface and Coatings Technology 204 (2010) 2230-2239.
[42] M. Balzer, M. Fenker, Three-dimensional thickness and property distribution of TiC films deposited by DC magnetron sputtering and HIPIMS, Surface and Coatings Technology 250 (2014) 37-43.
[43] K.-H. Grote, E.K. Antonsson, Springer handbook of mechanical engineering, Springer, Berlin (2009).
[44] W.C. Oliver, G.M. Pharr, An improved technique for determining hardness and elastic modulus using load and displacement sensing indentation experiments, Journal of Materials Research 7 (1992) 1564–1583.
[45] P. Colomban, S. Cherifi, G. Despert, Raman identification of corrosion products on automotive galvanized steel sheets, Journal of Raman Spectroscopy 39 (2008) 881-886.
[46] D. Uy, S.J. Simko, R.O. Carter III, R.K. Jensen, A.K. Gangopadhyay, Characterization of anti-wear films formed from fresh and aged engine oils, Wear 263 (2007) 1165-1174.
[47] H.C. Barshilia, N. Selvakumar, B. Deepthi, K.S. Rajam, A comparative study of reactive direct current magnetron sputtered CrAlN and CrN coatings, Surface and Coatings Technology 201 (2006) 2193-2201.
[48] H.C. Barshilia, K.S. Rajam, Raman spectroscopy studies on the thermal stability of TiN, CrN, TiAlN coatings and nanolayered TiN/CrN, TiAlN/CrN multilayer coatings, Journal of Materials Research 19 (2004) 3196-3205.
[49] A.E. Jiménez, A. Morina, A. Neville, M.D. Bermúdez, Surface interactions and tribochemistry in boundary lubrication of hypereutectic aluminium–silicon alloys, Proceedings of the Institution of Mechanical Engineers, Part J: Journal of Engineering Tribology 223 (2009) 593-601.
[50] B.C. Windom, W.G. Sawyer, D.W. Hahn, A Raman Spectroscopic Study of MoS_2 and MoO_3: Applications to Tribological Systems, Tribology Letters 42 (2011) 301-310.
[51] K. Mistry, A. Morina, A. Neville, Single cam tribometer for evaluating tribological parameters and tribochemistry of DLC coated valve train follower, Tribology - Materials Surfaces & Interfaces 6 (2012) 31-37.